Band-gap engineering with a twist: Formation of intercalant superlattices in twisted graphene bilayers

Franz Symalla,[1] Sam Shallcross,[2] Igor Beljakov,[1] Karin Fink,[1] Wolfgang Wenzel,[1] and Velimir Meded[1,*]

[1]*Institute of Nanotechnology, KIT, Karlsruhe, Hermann von Helmholtz-Platz 1, 76344 Eggenstein-Leopoldshafen, Germany*
[2]*Friedrich-Alexander-Universität Erlangen-Nürnberg, Staudtstrasse 7-B2, 91058 Erlangen, Germany*

Graphene-based materials have long been considered as promising building blocks for a new generation of high-frequency (terahertz) electronic devices, but their use is complicated by the lack of an intrinsic band gap in graphene itself. Here we exploit synthetically controllable incommensuration of twisted graphene bilayers as a scaffold for intercalation of alkali metal ions with the periodicity of the bilayer supercell. Systematic exploration of the energy profiles of the ions as a function of position suggests that the alkali metal ions aggregate commensurately with the symmetry of the twisted bilayer. The intercalated alkali metal ions act as a source of a periodic perturbation on the level of the bilayer supercell, which permits opening and engineering of a band gap between graphene's π bands. The twist angle between the graphene layers determines the structure and disorder of the intercalant sublattice and, consequently, the magnitude of the band gap. Appropriate choices of the intercalant and twist angle thus permit band-gap engineering in graphene. We offer arguments that the impact of intercalation on the all important charge mobility of graphene will be rather small.

I. INTRODUCTION

Since Novoselov and Geim [1] reported an electric field effect in exfoliated graphene, it has been heralded as a possible successor to silicon in high frequency semiconductor electronics [2–4]. Electron velocities of up to 10^6 m/s allow for potential clock rates of several hundred GHz [4] in graphene based transistors. However, harvesting these tremendous electron velocities for field effect transistors (FETs) requires a high on-off ratio, that is, a band gap significantly larger than room temperature to be created. Unfortunately, many of the methods, or theoretically suggested methods, to open a band gap in graphene do so at the expense of significantly reducing the effective electron velocities [2], thus limiting the frequency of graphene based FETs. The presentation of a scheme based on the twist graphene allotrope that may achieve both the desired band gap without obviously destroying the high mobility of graphene is the subject of this paper.

The creation of a band gap in graphene is achieved by coupling the π bands of graphene's two sublattices, which in the past has been accomplished in a number of different ways. In graphene nanoribbons the boundary conditions [2,3,5] open the gap, while on extended graphene sheets it can be achieved by chemical perturbation of the π network using hydrogenation [6], fluorination [7], removal of carbon atoms [8], or pressure augmented chemical interactions in multilayered graphene structures [9]. Band gaps have also been introduced through interactions with various substrates [10–12]. For graphene placed on metallic iridium [12] the gap is enhanced through patterned potassium adsorption on the iridium graphene superlattices. In graphene bilayer systems it can further be achieved by creation of an interlayer asymmetry either by surface doping [13] or a perpendicular electric field [14].

The fundamental problem to achieve graphenelike mobilities in band engineered graphene is posed by the disorder introduced by the perturbations, be this chemical disorder of either absorbents or vacancies, or by the edge disorder in a graphene nanoribbon. The presence of a substrate may also significantly reduce mobility via substrate-graphene interactions via, e.g., the presence of buffer layer states in the case of graphene on the Si face of SiC (0001). On the other hand, a modification of graphene on the crystal level—though avoiding intrinsic disorder—drastically changes the electronic properties [15,16].

For two graphene layers that have a mutual rotation, the graphene twist bilayer, this situation is different. For large angles the graphene twist bilayer exhibits a remarkable decoupling in a significant energy window about the Dirac point, such that the quasiparticle dynamics of the twist bilayer are essentially those of single layer graphene. In contrast to the case of single layer graphene, however, the twist bilayer comes with a natural energy landscape provided by the complex atomic structure of the twist bilayer unit cell. The unit cell of the bilayer features regions in which the two graphene layers are locally AA stacked, as well as regions in which the two layers are locally AB stacked (see Fig. 1). The former, due to their open geometry, present a much more favorable site for an interlayer impurity. This energy landscape, as we show, significantly suppresses the disorder that typically accompanies hybrid impurity-graphene systems, and thus allows for the geometry controlled functionalization of a graphene system. Additionally, the deleterious presence of a substrate may be excluded in the case of twist graphene stacks grown on the C face of SiC, where the SiC substrate is shielded from the graphene by 10–100 layers of mutually rotated graphene layers.

Furthermore, and most importantly, we show that intercalation of the twist bilayer by alkali and alkaline earth metals leads to the opening of a technologically significant band gap, while preserving the linear spectrum outside the gap. Given that impurity disorder is largely absent, disorder based

---
*Corresponding author: velimir.meded@kit.edu
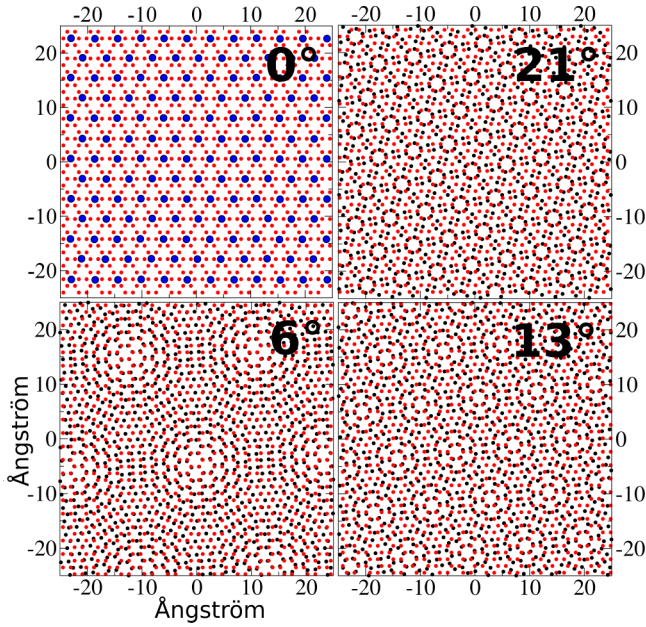
FIG. 1. (Color online) Moiré patterns of twisted graphene bilayers: Carbon atoms in bilayer graphene (red: top layer, black: bottom layer). Azimuthal rotation of two hexagonal lattices leads to superlattices of different size. The top left panel additionally shows the positions of Li intercalants (blue, bigger dots) in graphite.

mobility suppressing impurity scattering is expected to also be significantly reduced. This system therefore provides a highly promising hybrid graphene system for graphene FETs.

The remainder of the paper is structured as follows, first we present the computational methods deployed in this work, following which we then we then discuss the intercalation geometry in some detail. We subsequently focus on the electronic structure of the intercalated bilayers before concluding this paper.

II. COMPUTATIONAL METHODS

To determine the position of intercalated atoms in the bilayer, we have calculated their binding energy and intercalant-intercalant interactions using the plane wave based density functional theory (DFT) code VASP, using the projector augmented wave method (PAW) [17,18], and PB-GGA exchange-correlation functionals [19,20]. The Brillouin zone was sampled on special points according to Monkhorst and Pack [21]. The smallest 21° supercells were sampled on 41 weighted and Γ centered k points resulting from a $9 \times 9 \times 1$ subdivision along the reciprocal lattice vectors. The 27° and 13° supercells were sampled on a $5 \times 5 \times 1$ subdivided mesh, all bigger superlattices (>148 atoms) were sampled on a $3 \times 3 \times 1$ mesh. For the energy cutoff of the plane wave basis and the FFT mesh, redundant default settings from the PAW potentials supplied by VASP were used. To account for dispersion interactions, the empirical D2 dispersion potential of Grimme [22] was employed for both intercalant and graphene, using a global scaling factor of 0.75 and a damping factor of 20 [23].

III. INTERCALATION GEOMETRY

We first study the binding energies of the twisted graphene bilayer via DFT calculations. In the calculations of the binding energy minima of the intercalants we sample the sites between the bilayer retaining the symmetry between the two layers, which lie on lines in the real space unit cell, from which the neighboring carbon atoms from either graphene layer are equidistant as depicted in Fig. 2(a). The energy profiles for intercalation along those lines are shown for lithium, potassium, and calcium in a 27° twist angle bilayer, i.e., 52 carbon atoms per unit cell as depicted in Fig. 2(b). Qualitatively similar intercalation profiles are observed for all investigated alkali and alkaline earth species (Mg, Ca, Sr, Li, K, Na, Rb).
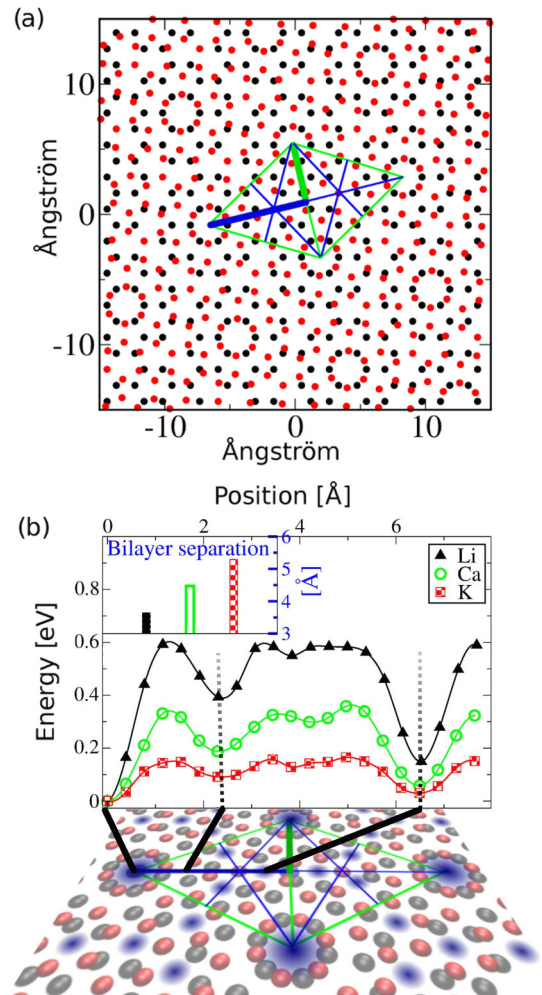
FIG. 2. (Color online) Deconstruction of the intercalation energy landscape: (a) Symmetry inequivalent lines used to calculate the energy profiles for intercalation in twisted bilayer graphene. Red and black dots defined as in Fig. 1, blue and green lines indicate symmetric positions with respect to top and bottom layers. Lines of equal color are equivalent. (b) Intercalation energies along the blue symmetry line for Li (black solid triangles), K (red checkered squares), and Ca (green open circles) in a 27° bilayer (primary minimum taken as the offset). Positions of primary and secondary energy minima are illustrated as shaded blue circles. The inset presents the graphene-graphene distance at the primary intercalation site in the intercalated bilayer for the respective intercalants.

A unique preferential site per unit cell exists between two matching carbon ring centers (the AA site). For a 27° twist angle the profile shows a secondary and tertiary minimum whose depths depend on intercalant size; the smaller the intercalant, the more pronounced the profile. Small intercalants resolve on a finer scale the structure of the bilayer, increasing the distinction between different intercalation sites. For Li the difference between the first neighboring minima is 0.4 eV in the 27° bilayer while it shrinks to 0.09 eV for K. In bilayers of small twist angles, such as the 6° bilayer shown in Fig. 1, favorable intercalation sites cluster around the AA center of a unit cell while regions between those centers have high-energy plateaus creating templates for spatially well separated 2D clusters of intercalates.

The intercalated alkali or alkaline earth atoms slightly buckle the bilayer around the intercalation site. The calculated interlayer distances at the apex of the buckles are thereby very similar to experimental interlayer distances [24,25] in (nontwisted) graphite intercalation compounds. The calculated twisted bilayer (experimental graphite intercalation compounds) interlayer distances at the intercalation site are for Li 3.7 (3.71) Å, for Na 4.5 (4.6) Å, and for K 5.3 (5.35) Å.

The diffusion barriers of the intercalant ions in the bilayer are validated against quantum Monte Carlo (QMC) calculations of Ganesh *et al.* [26] treating Li diffusion in AA stacked graphite. The diffusion barriers from the QMC calculations vary between 0.5 and 0.64 eV depending on the diffusion path. The diffusion barriers out of the primary minimum (the AA site) of a twisted bilayer are necessarily between these values, due to the broken mirror symmetry of the bilayer. In Fig. 2 we display a barrier of 0.6 eV for the diffusion of Li out of the AA site of the bilayer, which is within the energy interval obtained with QMC.

It is worth mentioning that in alkali intercalated (Bernal stacked) graphite a widening of interlayer distance proportional to the size of the intercalated atom is observed [25]. At low intercalant concentrations there is a local widening (bump) of the interlayer distance where an intercalant is placed, while the rest of the van der Waals heterostructure retains the interlayer spacing of the pristine bilayer system. Intercalation positions with a maximum cavity size are thus preferential in energy. In graphite alkali metal intercalation compounds this leads to rearrangement of the stacking order to a global AA stack, in which the intercalants sit between carbon rings [27]. Given the situation for intercalation preference, attested by not only our calculations but also by similar physics observed in graphite, we construct a simple heuristic model that includes the preference for intercalated atoms to the open lattice sites formulated in terms of distance of the intercalant, here the closed shell alkali metal ion, to the nearest carbon neighbor in the graphene bilayer with an offset and scaling according to $y = s(1/r - 1/r_0)$, where r_0 is the maximum distance to the closest carbon atom of all possible sites of the given bilayer and s is a single fit parameter to the DFT energies.

We show the power of this simplistic model in Fig. 3, where local lithium–nearest carbon distance maxima coincide with the location of all energy minima on the different sites as calculated with DFT. When applied to the symmetry lines of the supercells, the model reproduces the shape of the DFT intercalation energy potential quite accurately, see Fig. 3 where

the top and bottom rows are coming from DFT calculations along respective symmetry lines while the middle row is the two-dimensional (2D) plot coming from the simple model. Additionally, the model predicts for all the systems that were under study that all the intercalation energy minima within the supercell are located on the lines of symmetry, efficiently simplifying the DFT sampling of the potential energy surface, for the given twist angles, exclusively to the symmetry lines. This can be understood in terms of intercalants being furthest away from the neighboring carbon atoms of *both* graphene layers when being at the equidistant positions with respect to the same layers. However, it should be noted that this is not a general case and that deviations from this simple rule occur for bilayers with very small twist angle (i.e., large supercells).

Of course, after establishing the energetics of a single intercalated atom, we now proceed in the direction of intercalant-intercalant interactions, which are crucial for the determination of the equilibrium structure of an intercalated twist bilayer with a finite concentration of alkali/alkali earth intercalants. The optimal positions of the intercalated atoms in large lattices were calculated with a Metropolis Monte Carlo (MMC) scheme utilizing intercalant-intercalant repulsion from DFT. For this purpose we recalculated the energy profiles of Li in a bilayer for which the optimal (AA) position is already occupied by another Li intercalant. A Li atom was fixed in one of the two primary minima of two concatenated bilayer unit cells. The energy was then sampled for a second Li atom occupying a position along a symmetry line connecting to the other unit cell. The resulting profile matches the single intercalant profiles beyond an intercalant-intercalant distance of 4–5 Å, while there is repulsion between intercalants for smaller distances, see Fig. 4. This short range interaction can be attributed to Coulomb repulsion between charged neighboring intercalants and is effectively screened beyond ∼4 Å. The difference of the intercalation energy profiles of the first ion to the intercalation profiles of a second ion yields a distance dependent Li-Li repulsion that fits an exponential function $E_{\text{rep}}(d) = A_0 + A_1 e^{-A_2(d-A_3)}$ (see blue inset, Fig. 4). We use this effective interaction together with the single Li profiles to construct an effective energy model for the binding energies in lattices containing many intercalants.

Here we assume sites that are in local energy minima to be the only stable sites for the intercalants, so that possible equilibrium states of the intercalation compound are reduced to states in which every intercalant is in a local minimum, such that the intercalation energy for the intercalants can be written as

$$E_{\text{eff}} = \sum_s^{\text{sites}} o(s)E_{\text{site}} + \sum_{i,j}^{\text{intercalants}} E_{\text{rep}}(|r_i - r_j|),$$

$$o(s) = \begin{cases} s \text{ occupied} : 1, \\ s \text{ empty} : 0. \end{cases} \quad (1)$$

The site energies E_{sites} for single Li atoms are the minima illustrated as blue dots in Fig. 2, with more details in Fig. 3.

Using this energy model in a MMC scheme [28] we calculate the equilibrium distribution for a given density of intercalants in micron scale lattices. Figure 4 shows snapshots
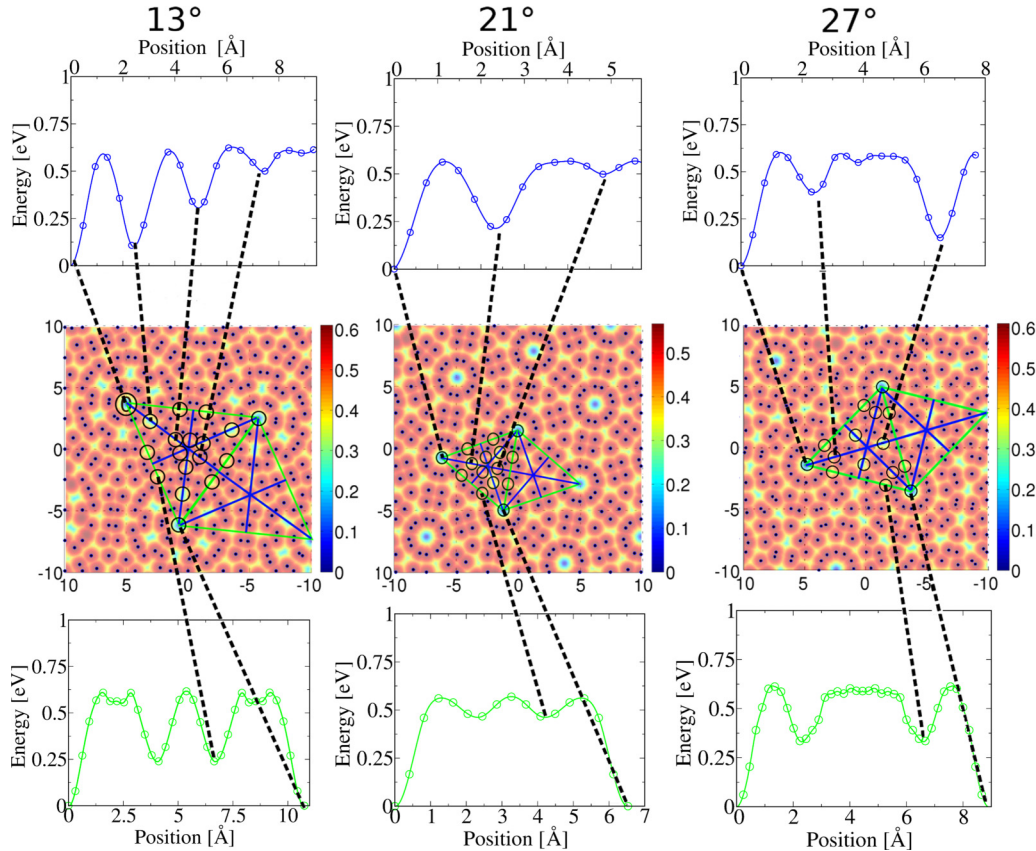
FIG. 3. (Color online) Intercalation energy landscape according to a geometrical model and DFT: On top and in the bottom the DFT energies sampled along first (blue, top) and second (green, bottom) symmetry line, from which all symmetry lines can be constructed. The color maps show the inverse distance to the closest carbon atom from the sites between the bilayer. Black circles mark the sites of local energy minima, which are predicted to lie exclusively on the lines of symmetry and agree in position with the DFT energy minima.

of resulting patterns for different twist angles and possible Li concentrations at 0 K.

The stability of these configurations at higher temperatures is quantified by the average number of intercalants offside their 0 K position per unit area [referred to as impurities in Fig. 4(d)]. The validity of this MMC approach is based on the assumption of ergodicity of the system. It is supported by recent experiments [29] with incommensurate bilayers of graphene/ruthenium as well as boron-nitride/rhodium, both topologically similar to our system, that show atoms which are injected into the bilayer to selectively settle at special sites in the superlattice, demonstrating the existence of diffusion mechanisms that bring the injected bilayer to an equilibrium state. We speculate that the diffusion through the bilayer supercell is aided by the phonon breathing modes of the weakly coupled van der Waals heterostructure, which can substantially widen the interlayer distance, ergo decrease the energy barriers for diffusion. Furthermore, as Vlaic *et al.* [30] show, that not defects but the interlayer potential originating from different rotational domains at the graphene/iridium interface indeed determine areas of, in their case, cobalt intercalation.

IV. ELECTRONIC STRUCTURE

Having established the structural configuration of the intercalated bilayer, we now discuss the impact that such

intercalation has on the electronic properties of the two decoupled layers of the twist bilayer. Intercalated with one alkali or alkaline earth atom per unit cell, the system exhibits a band structure rather similar to decoupled twisted bilayer graphene as the ionized intercalants are covalently inert and add no additional bands near the Fermi level. The donor electrons of the intercalants shift the Fermi level of the bilayer upwards depending on intercalant concentration and charge state, see Fig. 5(a), where the band structure of 9° bilayer (~150 C atoms in the unit cell) is displayed. The most significant effect is the opening of a band gap at the Dirac point presented in Figs. 5(a) and 5(b). It is caused by the sublattice coupling introduced within individual layers by the intercalants and independent of doping, as shown in the inset of Fig. 5(b), where the two excess electrons were removed from the calculation (jellium background compensated). The degeneracy of π and $\pi*$ cones of the top and bottom layers indicates the absence of hybridization between the π system and intercalant states, i.e., the preservation of aromaticity.

To use the system as a FET, the Fermi level has to be lowered to be close to the band gap. This is a similar situation to that which arises in the case of epitaxial graphene grown on the Si face of SiC for which the Fermi energy is displaced by approximately 0.3 eV from the Dirac point. Shifting the Fermi energy back to the Dirac point without deleteriously affecting the band structure has been demonstrated experimentally by
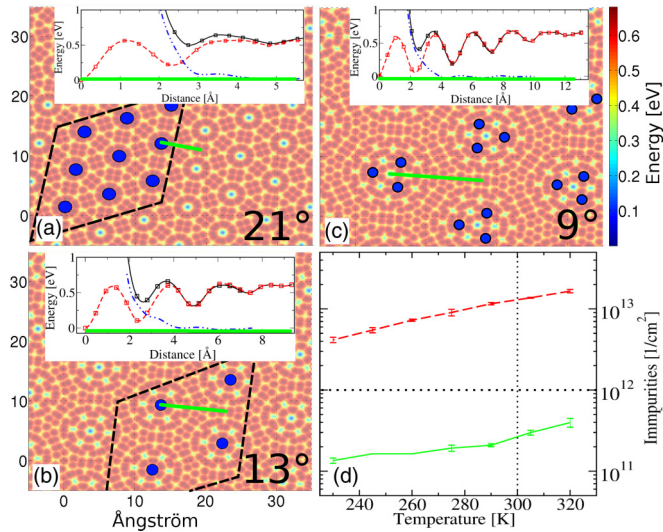
FIG. 4. (Color online) Intercalation patterns: (a)–(c) As blue dots, optimal intercalant distributions for intercalant concentrations of one per supercell for a 13° and 21° and three for a 9° bilayer. The insets show the Li binding energies for the first (red, dashed) intercalant, a second (black, solid) intercalant, and their effective repulsion (blue, dash-dot-dot) along the symmetry line (green). A reconstruction of the energy landscape is illustrated in the background. (d) Concentration of intercalants deviating from the optimal pattern as a function of temperature for the 21° (green, solid) and 13° (red, dashed) bilayers shown in (a) and (b). The dotted black straight line represents typical charge impurities from a substrate for comparison.

Lee *et al.* [31] by the deposition of a complex organic molecule on the graphene surface. A similar methodology is expected to work well for the case of the intercalated twist bilayer. To illustrate this via a simple "toy model" we decorate the bilayer with bromine, which is known to adsorb commensurate with the moiré pattern of similar systems [12], using a concentration of two bromine per alkali atom. The bromine atoms inject bands below the Dirac point, removing the excess electrons from the π bands but, importantly, preserving the band gap.

The width of the band gap can be tuned by the choice of both intercalant and twist angle. Experimentally, a wide range of twist angles have been observed and therefore accessing the full range of electronic features shown in Fig. 4 should be possible in the experiment. As a single intercalant per unit cell was chosen for all angles, an angle change also corresponds to a change in concentration. Figure 5(c) shows the band gaps (y axis) for Mg, Ca, Sr, Li, K, Na, and Rb as functions of the twist angle (lower x axis) or unit-cell size (upper x axis). We observe that the doubly charged alkaline earth ions open a wider band gap than the singly charged alkali metal ions. The highest band gaps are created for the highest concentrations of intercalants. We note that wider band gaps can be created with species forming stronger covalent bonds with carbon than alkali metals.

V. DISCUSSION AND CONCLUSION

Given a perfect sublattice of intercalants, transport properties of the intercalated twisted bilayer resemble those of the ideal bilayer, as the difference from the linear dispersion of the π bands can only be seen in a small interval of about ($\sim kT_{\text{Room}}$) above the edge of the bands. As the main scattering sources in pure graphene are charge impurities, it is to be expected that deviations of the charged intercalated ions from their optimal lattice sites might have a similarly important impact on electron mobility. To estimate effects on conductivity we employ the Boltzmann transport model of Hwang *et al.* [32] describing scattering in graphene on Coulomb charges. The linearity and degeneracy of the conducting π bands close to the Dirac point (Fig. 5) shows very weak coupling between the layers of the intercalated bilayer such that we assume that Hwang's model is also valid for conductivity estimation in the twisted bilayer. In his model the effect of charge impurities is estimated according to the linear dependence $\sigma = \text{const}\frac{n}{n_i}$ of the conductivity in graphene on the ratio of charge carriers n and charge impurities n_i [32]. A concentration of $10^{12}/\text{cm}^2$ substrate impurities is thereby required to reproduce the conductivity
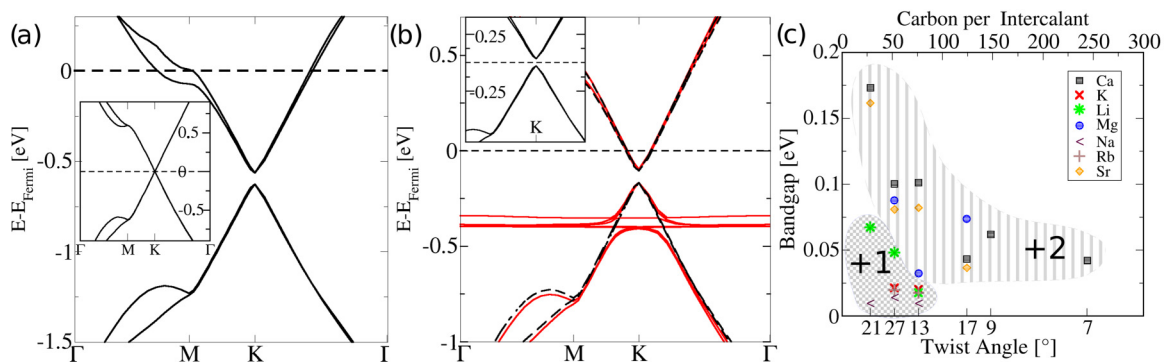
FIG. 5. (Color online) Electronic structure of alkali intercalated twisted bilayer graphene: (a) Band structure of a 9° bilayer intercalated with one Ca (electron configuration [Ar] $4s2$) atom per unit cell (inset without intercalation). Two $4s$ electrons are donated to the bilayer and shift the Fermi level up. Independently, a band gap is opened around the Dirac point, while the degeneracy of the bilayer bands is retained. (b) In red (solid) the bands of the intercalated bilayer additionally decorated with bromine. The flat bromine bands get populated by Ca $4s$ electrons lowering the Fermi level. Dashed black lines show the bands without bromine. The inset shows a preservation of the gap if the Ca $4s$ electrons are simply removed from the calculation (no Br involved). (c) Band gaps (y axis) for a number of intercalant species and twist angles (x axis), for a concentration of a single intercalant per unit cell. The largest band gap of 180 meV is achieved for Ca in 21° bilayer.

of an experimental graphene monolayer. The model is valid for $n_i < n$ and homogenous charge distributions, as would be given in a hypothetical on-state of a FET. Adding charged intercalants, the effective change in conductivity, assuming n_s charge impurities permanently present from the substrate and n_i charge impurities from the intercalation, is accordingly

$$\sigma_{i+s} = \sigma_s \frac{1}{1 + \frac{n_i}{n_s}}, \qquad (2)$$

where σ_s is the conductivity of the graphene in the presence of substrate charge impurities and σ_{s+i} is the conductivity including impurities of the intercalation. The number of impurities from the intercalation is taken from our MMC calculations while the number of substrate impurities was taken as constant at the value of $10^{-12}/cm^2$ which Hwang used. For a 21° (13°) bilayer, which in atoms per unit cell corresponds to 28 (76), intercalated with Li, the MMC predicts an increase by a factor of 1.2 (12.5) in the number of intercalation defects compared to the number of the postulated substrate impurities [Fig. 4(d)], which leads according to Eq. (2) to a decrease in conductivity by a factor of 0.8 (0.08). While only a rough estimate, it gives us an idea of what the cost of opening of a technologically relevant band gap in terms of charge transport properties could be.

In conclusion, we found that twisted graphene bilayers impose a pattern on intercalated atoms, resulting in a modification of the electronic properties of the hybrid materials. The intercalation of earth alkali atoms opens band gaps several times larger than room temperature without harming the symmetry of the graphene bilayers, which is crucial to minimize detrimental effects on its transport properties. While

intercalation of alkali metals and other species into nontwisted graphene bilayers [33] as well as graphite surfaces [34] and ultrathin graphite [35] has been experimentally demonstrated a substantial twist angle influence on electronic properties has been shown in experiment for other bilayer materials [36]. Annealing techniques could be used to systematically improve the periodicity of the intercalation, such that conductivities close to unmodified graphene might be achieved.

Electrostatic attraction of intercalated ions and the screening cloud in graphene stiffens the bilayer vertically, and might thereby quench phonon modes of top and bottom layers incommensurate with the supercell as well as increase the spring constant for flexural phonon modes [37], reducing sources for electron phonon or phonon mediated electron-electron scattering, thus further improve electron transport. These findings suggest that intercalated twisted graphene bilayers may be usable as high-mobility materials with appreciable band gaps. Further rich application potential could be opened by utilizing the high intercalant concentration periodic 2D nanocluster patterns (commensurate with the twisted bilayer supercell), where the twist angle determines both the shape and the intercluster distance. For example, magnetic 2D clusters could be relevant for, e.g., Kondo physics.

[1] K. S. Novoselov, A. K. Geim, S. V. Morozov, D. Jiang, Y. Zhang, S. V. Dubonos, I. V. Grigorieva, and A. A. Firsov, Science **306**, 666 (2004).

[2] F. Schwierz, Nat. Nanotechnol. **5**, 487 (2010).

[3] M. Schroter, M.Claus, P.Sakalas, D. Wang, and M. Haferlach, in *Proceedings of IEEE Bipolar/Bicmos Circuits and Technology Meeting* (IEEE, Portland, Oregon, 2012), pp. 112–119.

[4] L. Liao, Y.-C. Lin, M. Bao, R. Cheng, J. Bai, Y. Liu, Y. Qu, K. L. Wang, Y. Huang, and X. Duan, Nature (London) **467**, 305 (2010).

[5] J. Cai, P. Ruffieux, R. Jaafar, M. Bieri, T. Braun, S. Blankenburg, M. Muoth, A. P. Seitsonen, M. Saleh, X. Feng, K. Müllen, and R. Fasel, Nature (London) **466**, 470 (2010).

[6] R. Balog, B. Jørgensen, L. Nilsson, M. Andersen, E. Rienks, M. Bianchi, M. Fanetti, E. Lægsgaard, A. Baraldi, S. Lizzit, Z. Sljivancanin, F. Besenbacher, B. Hammer, T. G. Pedersen, P. Hofmann, and L. Hornekær, Nat. Mater. **9**, 315 (2010).

[7] A. R. Muniz and D. Maroudas, J. Phys. Chem. C **117**, 7315 (2013).

[8] F. Ouyang, S. Peng, Z. Liu, and Z. Liu, ACS Nano **5**, 4023 (2011).

[9] A. R. Muniz and D. Maroudas, J. Appl. Phys. **111**, 043513 (2012).

[10] S. Y. Zhou, G. H. Gweon, A. V. Fedorov, P. N. First, W. A. de Heer, D. H. Lee, F. Guinea, A. H. Castro Neto, and A. Lanzara, Nat. Mater. **6**, 770 (2007).

[11] B. Hunt, J. D. Sanchez-Yamagishi, A. F. Young, M. Yankowitz, B. J. LeRoy, K. Watanabe, T. Taniguchi, P. Moon, M. Koshino, P. Jarillo-Herrero, and R. C. Ashoori, Science **340**, 1427 (2013).

[12] M. Papagno, S. Rusponi, P. M. Sheverdyaeva, S. Vlaic, M. Etzkorn, D. Pacilé, P. Moras, C. Carbone, and H. Brune, ACS Nano **6**, 199 (2012).

[13] T. Ohta, A. Bostwick, T. Seyller, K. Horn, and E. Rotenberg, Science **313**, 951 (2006).

[14] Y. Zhang, T.-T. Tang, C. Girit, Z. Hao, M. C. Martin, A. Zettl, M. F. Crommie, Y. R. Shen, and F. Wang, Nature (London) **459**, 820 (2009).

[15] L. A. Chernozatonskii, P. B. Sorokin, A. G. Kvashnin, and D. G. Kvashnin, JETP Lett. **90**, 134 (2009).

[16] D. C. Elias, R. R. Nair, T. M. G. Mohiuddin, S. V. Morozov, P. Blake, M. P. Halsall, A. C. Ferrari, D. W. Boukhvalov, M. I. Katsnelson, A. K. Geim, and K. S. Novoselov, Science **323**, 610 (2009).

[17] G. Kresse and D. Joubert, Phys. Rev. B **59**, 1758 (1999).

[18] P. E. Blöchl, Phys. Rev. B **50**, 17953 (1994).

[19] J. P. Perdew, K. Burke, and M. Ernzerhof, Phys. Rev. Lett. **77**, 3865 (1996).

[20] J. P. Perdew, K. Burke, and M. Ernzerhof, Phys. Rev. Lett. **78**, 1396 (1997).

[21] H. J. Monkhorst and J. D. Pack, Phys. Rev. B **13**, 5188 (1976).

[22] S. Grimme, J. Comput. Chem. **27**, 1787 (2006).

[23] T. Bucko, J. Hafner, S. Lebegue, and J. G. Angyan, J. Phys. Chem. A **114**, 11814 (2010).

[24] D. Guerard and A. Herold, Carbon **13**, 337 (1975).

[25] T. Enoki, M. Suzuki, and M. Endo, *Graphite Intercalation Compounds and Applications* (Oxford University Press, Oxford, 2003).

[26] P. Ganesh, J. Kim, C. Park, M. Yoon, F. A. Reboredo, and P. R. C. Kent, J. Chem. Theory Comput. **10**, 5318 (2014).

[27] J. E. Fischer and T. E. Thompson, Phys. Today **31**, 36 (2008).

[28] N. Metropolis, A. W. Rosenbluth, M. N. Rosenbluth, A. H. Teller, and E. Teller, J. Chem. Phys. **21**, 1087 (1953).

[29] H. Cun, M. Iannuzzi, A. Hemmi, S. Roth, J. Osterwalder, and T. Greber, Nano Lett. **13**, 2098 (2013).

[30] S. Vlaic, A. Kimouche, J. Coraux, B. Santos, A. Locatelli, and N. Rougemaille, Appl. Phys. Lett. **104**, 101602 (2014).

[31] D. S. Lee, C. Riedl, T. Beringer, A. H. Castro Neto, K. von Klitzing, U. Starke, and J. H. Smet, Phys. Rev. Lett. **107**, 216602 (2011).

[32] E. H. Hwang, S. Adam, and S. Das Sarma, Phys. Rev. Lett. **98**, 186806 (2007).

[33] N. Kim, K. S. Kim, N. Jung, L. Brus, and P. Kim, Nano Lett. **11**, 860 (2011).

[34] A. Nagashima, N. Tejima, and C. Oshima, Phys. Rev. B **50**, 17487 (1994).

[35] W. Bao, J. Wan, X. Han, X. Cai, H. Zhu, D. Kim, D. Ma, Y. Xu, J. N. Munday, H. D. Drew, M. S. Fuhrer, and L. Hu, Nat. Commun. **5**, 4224 (2014).

[36] A. M. van der Zande, J. Kunstmann, A. Chernikov, D. A. Chenet, Y. You, X. Zhang, P. Y. Huang, T. C. Berkelbach, L. Wang, F. Zhang, M. S. Hybertsen, D. A. Muller, D. R. Reichman, T. F. Heinz, and J. C. Hone, Nano Lett. **14**, 3869 (2014).

[37] A. M. Shikin, G. V. Prudnikova, V. K. Adamchuk, F. Moresco, and K. H. Rieder, Phys. Rev. B **62**, 13202 (2000).